Single-phonon and multi-phonon excitations of the γ vibration in rotating odd-A nuclei

Masayuki Matsuzaki*

Department of Physics, Fukuoka University of Education,

Munakata, Fukuoka 811-4192, Japan

(Dated: October 21, 2014)

arXiv:1406.3445v2 [nucl-th] 20 Oct 2014

Abstract

Background Collective motions in quantum many-body systems are described as bosonic excitations. Multi-phonon excitations in atomic nuclei, however, were observed very rarely. In particular, the first two-phonon γ vibrational (2γ) excitation in odd-A nuclei was reported in 2006 and only a few have been known so far. Two theoretical calculations for the data on ^{103}Nb were performed, one of which was done by the present author within a limited model space up to 2γ basis states. Quite recently, conspicuously enhanced $B(E2)$s, reduced $E2$ transition probabilities, feeding 2γ states were observed in ^{105}Nb and conjectured that their parent states, called band (4), are candidates of 3γ states.

Purpose In the present work, the model space is enlarged up to 4γ basis states. The purpose is twofold: One is to see how the description of 2γ eigenstates in the previous work is improved, and the other is to examine the existence of collective 3γ eigenstates, and when they exist, study their collectivity through calculating interband $B(E2)$s.

Method The particle-vibration coupling model based on the cranking model and the random-phase approximation is used to calculate the vibrational states in rotating odd-A nuclei. Interband $B(E2)$s are calculated by adopting the method of the generalized intensity relation.

Results The present model reproduces well the energy spectra and $B(E2)$s of 0γ – 2γ states in ^{103}Nb and ^{105}Nb. For 3γ states, calculated spectra indicate that the most collective state with the highest K at zero rotation feels strong Coriolis force after rotation sets in and consequently is observed with lowered K, where K is the projection of the angular momentum to the z axis. The calculated states account for the observed enhanced $B(E2)$s within factors of 2 – 3.

Conclusions The present calculation with the enlarged model space reproduces the observed 0γ – 2γ states well and predicts properties of collective 3γ states. The most collective one is thought to be the main component of the observed band (4) from the analyses of the energy spectra and interband $B(E2)$s although some mixing with states that are not included in the present model would be possible.

PACS numbers: 21.10.Re, 21.60.Jz, 27.60.+j

*matsuza@fukuoka-edu.ac.jp

I. INTRODUCTION

Collective motions in quantum many-body systems are formed as coherent superpositions of many individual degrees of freedom, and are described as bosonic excitations. In atomic nuclei, one of finite many-body systems, the representative is vibrations of the surface of the average potential produced self-consistently to the nucleon distribution. However, repeated excitations, the characteristic of bosons, are not always observed. Even when observed, their strengths spread over many eigenstates because collective and individual noncollective excitations have similar energy scale. Therefore, existence and properties of multiple excitations have been a longstanding subject of theoretical and experimental studies.

Famous examples are known in high-lying giant resonances. Double excitations of the one with the same multipole and of different types have been observed; see for example, a review [1]. Among low-lying vibrations, the multi-phonon quadrupole vibrational states in spherical nuclei have long been studied around ^{110}Cd [2, 3]. In axially symmetric or weakly triaxial deformed nuclei, the two-phonon γ vibration, denoted as 2γ hereafter, was studied for three decades as concisely reviewed in Ref. [4], but observed only in ^{168}Er, ^{166}Er, ^{164}Dy, ^{232}Th, ^{106}Mo and ^{104}Mo in even-even nuclei. Recently, another candidate was reported in the weakly deformed, γ-soft nucleus, ^{138}Nd [5].

In odd-A nuclei, vibrations of the average potential alter the particle motion and the change thus caused affects back the average potential. Consequently the particle motion and the vibration couple to each other to various degrees. This coupling makes the excitation spectrum complex in general. From another point of view, however, a stretched parallel coupling of the high-j particle and $K = 2$ phonons can produce high-K states that can hardly mix with other states with lower K. Here j is the single-particle angular momentum, and $K = 2$ the projection to the z axis of the angular momentum carried by the γ vibration. Accordingly there can be more opportunities to observe multi-phonon γ-vibrational states.

Prior to experimental observations, numerical predictions for odd-A nuclei were made in Ref. [6]. The first observation was made 10 years later in ^{105}Mo [7]. Soon after this, similar bands were observed in ^{103}Nb [8] and in ^{107}Tc [9]. The first realistic theoretical calculation in terms of the triaxial projected shell model was reported for ^{103}Nb [10] in 2010. The calculation in terms of the particle-vibration coupling (PVC) model based on the cranking model and the random-phase approximation (RPA) was done in 2011 [4].

As another type of multi-phonon state in strongly triaxial deformed nuclei, two-phonon wobbling bands were observed in ^{163}Lu [11] and ^{165}Lu [12] and analyzed in Ref. [13]. Furthermore, the rotational bands built on the high-K multi-quasiparticle states can be interpreted theoretically as a multi-phonon excitation of the precession mode, which is the axially-symmetric limit of the wobbling mode [14].

Quite recently, a 2γ band in ^{105}Nb bearing much resemblance to that in ^{103}Nb was reported [15]. The characteristic feature common to these two isotopes but beyond the scope of Ref. [4] is that the observed band (4) is interpreted as a candidate of the 3γ band. In particular in ^{105}Nb, $B(E2)$s from this band to the 2γ band are conspicuously enhanced compared with the Weisskopf unit.

In Ref. [4], the model, which was developed to study the signature dependence in 0γ bands in the rare-earth region [16, 17] and utilized later to study the two sequences with $K = \Omega \pm 2$ of the 1γ band in ^{165}Ho and the one with $K = \Omega + 2$ in ^{167}Er [18], was applied to the 2γ band for the first time. Here Ω is the projection of the single-particle angular momentum to the z axis. From a microscopic many-body theoretical point of view, the mechanism that leads to anharmonicity of the spectrum beyond the RPA was discussed in the studies of 2γ bands in even-even nuclei [19], however, the present model concentrates on that peculiar to odd-A systems. The result was that the 0γ and 1γ bands were reproduced perfectly but the calculated 2γ band was somewhat higher in energy than the observed one as in the other calculation [10].

In the present paper, the model space is enlarged up to 4γ basis states and the interband $B(E2)$s are also calculated utilizing the method of the generalized intensity relation (GIR) [2, 20]. The purpose is twofold: One is to see how the description of 2γ states in Ref. [4] is improved, and the other is to look into the existence of 3γ states, and when they exist, study their collectivity through calculating vibrational $B(E2)$s. This is the first attempt to study realistic 3γ states in deformed nuclei, to the author's knowledge.

Throughout this paper the $\hbar = 1$ unit is used.

II. THE MODEL

A. Particle-vibration coupling

Eigenstates of the odd-A nucleus in a rotating frame are calculated in the particle-vibration coupling model based on the cranking model and the RPA. The adopted Hamiltonian is the same as in Ref. [4], therefore recapitulated only briefly here. The detailed definitions of the adopted notations were given there [4]. I begin with the cranked Nilsson plus BCS one-body Hamiltonian,

$$h' = h - \omega_{\rm rot} J_x, \tag{1}$$

$$h = h_{\rm Nil} - \Delta_\tau (P_\tau^\dagger + P_\tau) - \lambda_\tau N_\tau, \tag{2}$$

$$h_{\rm Nil} = \frac{\mathbf{p}^2}{2M} + \frac{1}{2} M(\omega_x^2 x^2 + \omega_y^2 y^2 + \omega_z^2 z^2) + v_{ls} \mathbf{l}\cdot\mathbf{s} + v_{ll}(\mathbf{l}^2 - \langle \mathbf{l}^2 \rangle_{N_{\rm osc}}). \tag{3}$$

This Hamiltonian gives quasiparticle states created by $a_\mu^\dagger$ and $a_{\bar\mu}^\dagger$ with signature $r = \exp(-i\pi\alpha) = -i$ and $+i$, respectively. Then I apply the RPA to the residual pairing plus doubly-stretched quadrupole-quadrupole interaction between quasiparticles. The interaction Hamiltonian is given by

$$H_{\rm int} = -\sum_{\tau=1,2} G_\tau \tilde{P}_\tau^\dagger \tilde{P}_\tau - \frac{1}{2} \sum_{K=0,1,2} \kappa_K^{(+)} Q_K''^{(+)\dagger} Q_K''^{(+)} - \frac{1}{2} \sum_{K=1,2} \kappa_K^{(-)} Q_K''^{(-)\dagger} Q_K''^{(-)}, \tag{4}$$

where $Q_K''^{(\pm)}$ are the signature-coupled form of the quadrupole operators defined by the doubly-stretched coordinates.

Among the RPA modes, $X_n^\dagger$, determined by $H_{\rm int}$, I choose the γ-vibrational phonons, $n = \gamma(\pm)$ with signature $r = \pm 1$, which have outstandingly large $K = 2$ transition amplitudes. In terms of the quasiparticles and the γ-vibrational phonons thus determined, the particle-vibration coupling Hamiltonian takes the form

$$\begin{aligned} H_{\rm couple}(\gamma) = & \sum_{\mu\nu} \Lambda_{\gamma(+)}(\mu\nu) \left(X_{\gamma(+)}^\dagger a_\mu^\dagger a_\nu + X_{\gamma(+)} a_\nu^\dagger a_\mu \right) \\ & + \sum_{\mu\bar\nu} \Lambda_{\gamma(-)}(\mu\bar\nu) \left(X_{\gamma(-)}^\dagger a_\mu^\dagger a_{\bar\nu} + X_{\gamma(-)} a_{\bar\nu}^\dagger a_\mu \right) \\ & + \text{sig. conj.} \end{aligned} \tag{5}$$

The coupling vertices are given by

$$\Lambda_{\gamma(+)}(\mu\nu) = -\sum_{K=0,1,2} \kappa_K^{(+)} T_K''^{(+)} Q_K''^{(+)}(\mu\nu),$$
$$\Lambda_{\gamma(-)}(\mu\bar{\nu}) = -\sum_{K=1,2} \kappa_K^{(-)} T_K''^{(-)} Q_K''^{(-)}(\mu\bar{\nu}), \tag{6}$$
$$\text{and sig. conj.,}$$

where $T_K''^{(\pm)}$ are the doubly-stretched quadrupole transition amplitudes associated with the γ-vibrational phonons and $Q_K''^{(\pm)}(\alpha\beta)$ denote quasiparticle scattering matrix elements.

Eigenstates of the total Hamiltonian at each $\omega_{\rm rot}$ take the form

$$\begin{aligned}
|\chi_i\rangle = & \sum_\mu \psi_i^{(1)}(\mu)\, a_\mu^\dagger |\phi\rangle \\
& + \sum_\mu \psi_i^{(3)}(\mu\gamma)\, a_\mu^\dagger X_\gamma^\dagger |\phi\rangle + \sum_{\bar\mu} \psi_i^{(3)}(\bar\mu\bar\gamma)\, a_{\bar\mu}^\dagger X_{\bar\gamma}^\dagger |\phi\rangle \Big\rangle \\
& + \sum_\mu \psi_i^{(5)}(\mu\gamma\gamma) \frac{1}{\sqrt{2}}\, a_\mu^\dagger (X_\gamma^\dagger)^2 |\phi\rangle + \sum_\mu \psi_i^{(5)}(\mu\bar\gamma\bar\gamma) \frac{1}{\sqrt{2}}\, a_\mu^\dagger (X_{\bar\gamma}^\dagger)^2 |\phi\rangle \Big\rangle \\
& + \sum_{\bar\mu} \psi_i^{(5)}(\bar\mu\gamma\bar\gamma)\, a_{\bar\mu}^\dagger X_\gamma^\dagger X_{\bar\gamma}^\dagger |\phi\rangle \Big\rangle \\
& + \sum_\mu \psi_i^{(7)}(\mu\gamma\gamma\gamma) \frac{1}{\sqrt{3!}}\, a_\mu^\dagger (X_\gamma^\dagger)^3 |\phi\rangle + \sum_{\bar\mu} \psi_i^{(7)}(\bar\mu\bar\gamma\bar\gamma\bar\gamma) \frac{1}{\sqrt{3!}}\, a_{\bar\mu}^\dagger (X_{\bar\gamma}^\dagger)^3 |\phi\rangle \Big\rangle \\
& + \sum_{\bar\mu} \psi_i^{(7)}(\bar\mu\gamma\gamma\bar\gamma) \frac{1}{\sqrt{2}}\, a_{\bar\mu}^\dagger (X_\gamma^\dagger)^2 X_{\bar\gamma}^\dagger |\phi\rangle \Big\rangle + \sum_\mu \psi_i^{(7)}(\mu\gamma\bar\gamma\bar\gamma) \frac{1}{\sqrt{2}}\, a_\mu^\dagger X_{\bar\gamma}^\dagger (X_{\bar\gamma}^\dagger)^2 |\phi\rangle \Big\rangle \\
& + \sum_\mu \psi_i^{(9)}(\mu\gamma\gamma\gamma\gamma) \frac{1}{\sqrt{4!}}\, a_\mu^\dagger (X_\gamma^\dagger)^4 |\phi\rangle + \sum_\mu \psi_i^{(9)}(\mu\bar\gamma\bar\gamma\bar\gamma\bar\gamma) \frac{1}{\sqrt{4!}}\, a_\mu^\dagger (X_{\bar\gamma}^\dagger)^4 |\phi\rangle \Big\rangle \\
& + \sum_{\bar\mu} \psi_i^{(9)}(\bar\mu\gamma\gamma\gamma\bar\gamma) \frac{1}{\sqrt{3!}}\, a_{\bar\mu}^\dagger (X_\gamma^\dagger)^3 X_{\bar\gamma}^\dagger |\phi\rangle \Big\rangle + \sum_{\bar\mu} \psi_i^{(9)}(\bar\mu\gamma\bar\gamma\bar\gamma\bar\gamma) \frac{1}{\sqrt{3!}}\, a_{\bar\mu}^\dagger X_\gamma^\dagger (X_{\bar\gamma}^\dagger)^3 |\phi\rangle \Big\rangle \\
& + \sum_\mu \psi_i^{(9)}(\mu\gamma\gamma\bar\gamma\bar\gamma) \frac{1}{2}\, a_\mu^\dagger (X_\gamma^\dagger)^2 (X_{\bar\gamma}^\dagger)^2 |\phi\rangle \Big\rangle ,
\end{aligned} \tag{7}$$

for the $r = -i$ sector,

where γ and $\bar\gamma$ abbreviate $\gamma(+)$ and $\gamma(-)$, respectively, and $|\phi\rangle$ is the rotating vacuum configuration. Those for the $r = +i$ sector take a similar form. This notation indicates that a limited class of 1, 3, 5, 7, and 9qp states that contribute to multi-phonon γ-vibrational states are taken into account. Among these, the model space was truncated up to the $\psi^{(5)}$ terms in Ref. [4]. Here it should be noted that the tilt of the rotational axis brought about by large triaxial deformations can mix signature quantum number in general. But the

rotation is essentially one-dimensional when the static triaxial deformation is smaller than the zero-point amplitude of the γ vibration.

B. Generalized intensity relation

The rotational effects on the vibrational (interband) transition rates are well described by the generalized intensity relation in terms of the intrinsic matrix elements, see Fig. 4-30 in Ref. [2]. On the other hand, the cranking model and its extensions can provide us with rotationally perturbed intrinsic matrix elements precisely. Therefore, a method to combine these two was proposed in Ref. [20] and applied to the $1\gamma \to 0\gamma$ transitions in ^{165}Ho and ^{167}Er in Ref. [18]. In the present study, this method is applied to the $n\gamma \to (n-1)\gamma$ transitions with n =1, 2, and 3, along the way of this reference. The expressions for the $B(E2)$ are

$$B(E2 : I_\mathrm{i}K_\mathrm{i} \to I_\mathrm{f}K_\mathrm{f}) = \langle I_\mathrm{i}K_\mathrm{i}2\Delta K|I_\mathrm{f}K_\mathrm{f}\rangle^2 Q_\mathrm{out}^2, \tag{8}$$

$$Q_\mathrm{out} = Q_1 + Q_2[I_\mathrm{f}(I_\mathrm{f}+1) - I_\mathrm{i}(I_\mathrm{i}+1)], \tag{9}$$

$$Q_1 = \sqrt{2}Q_\mathrm{tr} - \Delta K(K_\mathrm{i}+K_\mathrm{f})Q_2, \tag{10}$$

$$Q_\mathrm{tr} = \langle \mathrm{f}|Q_2^{(+)}|\mathrm{i}\rangle, \tag{11}$$

$$Q_2 = \frac{1}{\sqrt{2}\mathcal{J}}\frac{\mathrm{d}\langle \mathrm{f}|Q_1^{(+)}|\mathrm{i}\rangle}{\mathrm{d}\omega_\mathrm{rot}}, \tag{12}$$

where Q_tr and Q_2 are evaluated at $\omega_\mathrm{rot} = 0$, and the moment of inertia, $\mathcal{J}$, is extracted from the experimental energy of the first $\Delta I = 2$ excited states in the ground band.

III. RESULTS AND DISCUSSION

Numerical calculations are performed for two isotopes, ^{103}Nb and ^{105}Nb, in which candidates of 3γ states were observed [8, 15]. The former was investigated in Ref. [4] within a limited model space, and the latter, on which the data were reported quite recently, is newly studied. In both isotopes, the ground band is based on the $\pi[422]\,5/2^+$ asymptotic state, and the single- and multi-phonon γ-vibrational excitations on top of it were observed. Cranking and RPA calculations are done in the five major shells, $N_\mathrm{osc} = 2$ – 6 for the neutron and 1 - 5 for the proton. The indices μ and $\bar{\mu}$ in Eq. (7) for the PVC eigenstates run from 1 to 15, the number of quasiparticle states with $N_\mathrm{osc} = 4$. In the following, the results for the

favored signature, $r = -i$, are mainly presented while those for the unfavored $r = +i$ are also shown when necessary.

A. $0\gamma - 2\gamma$ states in ^{103}Nb

All the parameters entering into the calculation are the same as those adopted in Ref. [4]. The pairing gaps $\Delta_n = 1.05$ MeV, $\Delta_p = 0.85$ MeV and the deformation $\epsilon_2 = 0.31$ are adopted conforming to the experimental analyses [8, 21]. The triaxiality $\gamma = -7^\circ$ is chosen to reproduce the measured signature splitting of the ground band in the PVC calculation. The quadrupole force strengths are determined to reproduce in the axially symmetric limit the γ-vibrational energy observed in ^{104}Mo [22], see Ref. [4] for the detail.

1. Distribution of collective states

In Fig. 1, the distribution of collective states are shown. In the following, I denote the favored signature of the lowest quasiparticle state as $1qp$, and its signature partner as $\overline{1qp}$. The lowest PVC eigenstate whose main component is this $1qp$ is often denoted also as the 0γ state. Then the fraction of the 1γ components (green dashed in the figure) means the sum of the probabilities of $1qp \otimes \gamma(+)$ and $\overline{1qp} \otimes \gamma(-)$ basis states. The conventions for multi-phonon states are understood straightforwardly.

At $\omega_{\rm rot} = 0$, $0\gamma - 3\gamma$ states are almost harmonic, whereas the 4γ strength is located higher than the harmonic location. In addition, the main peaks of $0\gamma - 4\gamma$ states are almost of the same height although the collective strength spreads as the number of phonon increases. As discussed later, the main peaks have fairly pure K.

As soon as rotation sets in, the heights of the main peaks decrease approximately in proportion to the number of phonon. Two sequences of 1γ and three sequences of 2γ states survive up to high spins as discussed in Ref. [4]. In addition, three or four sequences of 3γ states keep their collective character to some extent. Routhians of $n\gamma$ states are $e'_{2\gamma} < e'_{0\gamma} + 2\Delta_p$, but $e'_{0\gamma} + 2\Delta_p < e'_{3\gamma} < e'_{0\gamma} + 2\Delta_n$. Therefore, the collectivity of the calculated 3γ states other than high-K ones, which are hard to mix with other states, should be considered with reservations, because in the present model $1qp \otimes 3\gamma$ basis states couple only with $(1\mathrm{qp})' \otimes 2\gamma$ and $(1\mathrm{qp})' \otimes 4\gamma$, whereas direct couplings to 3qp states are not

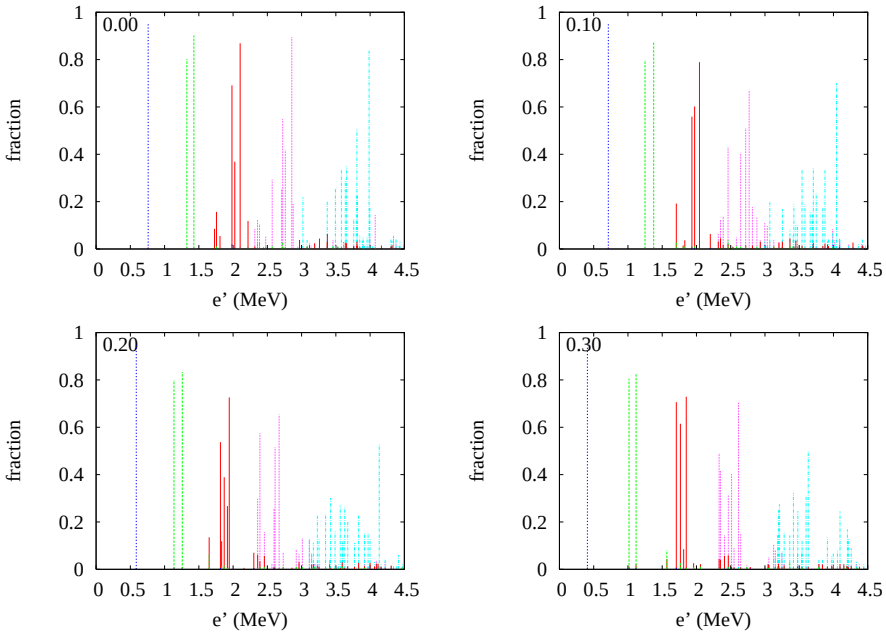

FIG. 1: (Color online) Distribution of the collective fraction (probability in the wave function) of the 0γ, 1γ, 2γ, 3γ, and 4γ components in the favored signature ($r = -i$) sector of ^{103}Nb, $|\psi^{(1)}(1)|^2$ (blue longer dotted), $|\psi^{(3)}(1\gamma)|^2 + |\psi^{(3)}(\bar{1}\bar{\gamma})|^2$ (green dashed), $|\psi^{(5)}(1\gamma\gamma)|^2 + |\psi^{(5)}(1\bar{\gamma}\bar{\gamma})|^2 + |\psi^{(5)}(\bar{1}\gamma\bar{\gamma})|^2$ (red solid), $|\psi^{(7)}(1\gamma\gamma\gamma)|^2 + |\psi^{(7)}(\bar{1}\bar{\gamma}\bar{\gamma}\bar{\gamma})|^2 + |\psi^{(7)}(\bar{1}\gamma\gamma\bar{\gamma})|^2 + |\psi^{(7)}(1\gamma\bar{\gamma}\bar{\gamma})|^2$ (magenta dotted), and $|\psi^{(9)}(1\gamma\gamma\gamma\gamma)|^2 + |\psi^{(9)}(1\bar{\gamma}\bar{\gamma}\bar{\gamma}\bar{\gamma})|^2 + |\psi^{(9)}(\bar{1}\gamma\gamma\gamma\bar{\gamma})|^2 + |\psi^{(9)}(\bar{1}\gamma\bar{\gamma}\bar{\gamma}\bar{\gamma})|^2 + |\psi^{(9)}(1\gamma\gamma\bar{\gamma}\bar{\gamma})|^2$ (blue dot-dashed), respectively, at $\omega_{\rm rot} = 0$ – 0.3 MeV.

included, where $(1\mathrm{qp})'$ denotes other one-quasiparticle basis states including those of the opposite signature.

In Fig. 2, calculated eigenstates in the regions of (a) 1γ and (b) 2γ states are shown. Among them, those with more than 50% collective (1γ or 2γ) fraction are emphasized with red crosses. The two 1γ sequences are completely isolated from other states. The three 2γ ones are also distinguished from other states but crossed by two up-slope noncollective states at around $\omega_{\rm rot} = 0.15$ – 0.2 MeV.

2. *Characterization of the calculated* 1γ *and* 2γ *states*

On the correspondence between 1γ bands in the calculation in the signature scheme and that in the K scheme, it was argued in Ref. [4] that the obtained lower band can be identified with the $K = \Omega - 2$ band because states with lower K have lower intrinsic energies than those

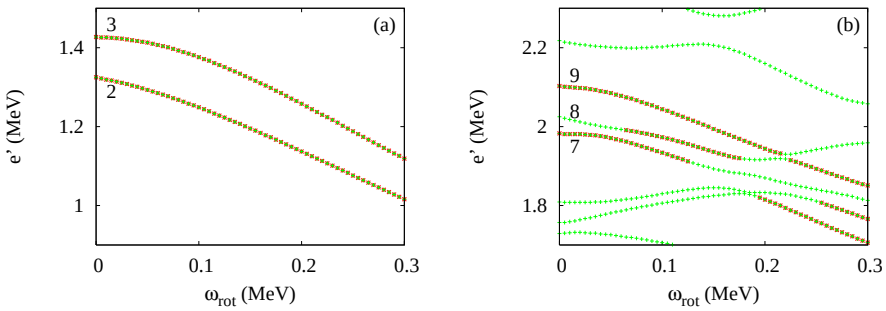

FIG. 2: (Color online) Routhians of all calculated PVC states in the $r = -i$ sector of ^{103}Nb in the regions of (a) 1γ and (b) 2γ bands are shown by green +s. Those with more than 50% collective fraction are emphasized by red $\times$s. The labels attached designate the numbers, i in Eq. (7), enumerated from the lowest.

with higher K and the same total angular momentum I. To look into this correspondence more, the aligned angular momenta around $\omega_{\rm rot} = 0$ are shown in Figs. 3 (a) for 1γ and (b) for 2γ states. The labels i of states refer to those in Fig. 2.

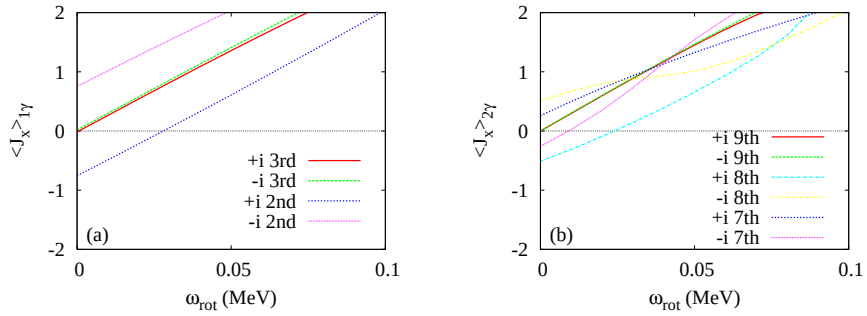

FIG. 3: (Color online) Expectation values of the projection of the angular momentum to the rotational (x) axis around the band heads of (a) 1γ and (b) 2γ bands in ^{103}Nb.

The 1γ band should have $K = |\Omega - 2| = 1/2$ or $\Omega + 2 = 9/2$ at the band head aside from weak K mixing stemming from static triaxial deformation. Figure 3(a) clearly shows that the lower (second) pair of states has a strong signature decoupling, non-zero aligned angular momentum with opposite sign at $\omega_{\rm rot} = 0$, while the upper (third) pair has practically zero aligned angular momentum at $\omega_{\rm rot} = 0$ and negligible signature splitting. This proves the mapping that the lower band is of low K and the upper band is of high K.

The characterization is further evidenced by looking at the wave function. Figure 4 graphs the amplitudes of the dominant components, $D(+) = |\psi_i^{(3)}(1\gamma)|$ for $1qp \otimes \gamma(+)$ and

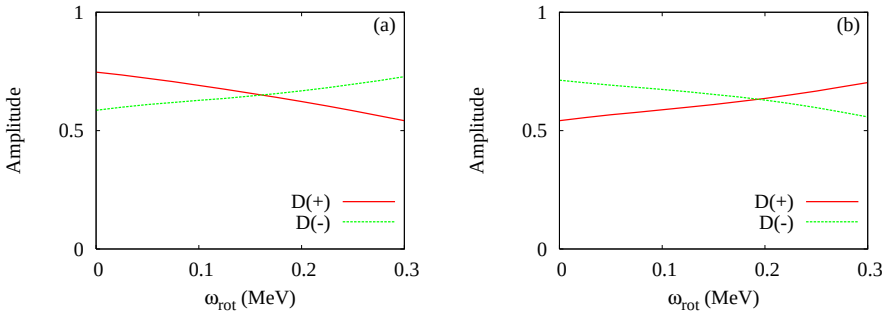

FIG. 4: (Color online) Amplitudes of the dominant components $D(+) = |\psi_i^{(3)}(1\gamma)|$ and $D(-) = |\psi_i^{(3)}(\bar{1}\bar{\gamma})|$ in (a) upper (i = 3rd) and (b) lower (i = 2nd) 1γ bands in the $r = -i$ sector of ^{103}Nb.

$D(-) = |\psi_i^{(3)}(\bar{1}\bar{\gamma})|$ for $\overline{1qp} \otimes \gamma(-)$, in (a) upper ($i$ = 3rd) and (b) lower (i = 2nd) bands. The structure of the $\gamma(\pm)$ is $(Q_{22} \pm Q_{2-2})/\sqrt{2}$. These two components mix with similar magnitudes both in the upper and lower eigenstates and their relative sign (not shown) is always opposite. This means that the two orthogonal combinations of $\gamma(\pm)$ reproduce high-K and low-K states.

The 2γ band should have $K = |\Omega - 4| = 3/2$ or $\Omega = 5/2$ or $\Omega + 4 = 13/2$ at the band head. An argument for Fig. 3(b) similar to that for 1γ bands in Fig. 3(a) leads to the identification that the ninth pair is $K = 13/2$, the eighth and seventh are $K = 3/2$ and $K = 5/2$. The latter two interact with each other in $r = -i$ as soon as rotation sets in. This interaction can also be seen in Fig. 2(b). Note that the eighth state has about 35% collectivity at $\omega_{\rm rot} = 0$ but it increases as $\omega_{\rm rot}$ increases.

This discussion confirms that the calculated upper bands, third for 1γ and ninth for 2γ, possess the character of the highest K, $K = 9/2$ and $13/2$, respectively. Because the observed bands (2) and (3) were assigned experimentally as $K = 9/2$ and $13/2$, respectively, the correspondence between the theory and experiment is established. This is natural in that the most collective state with less mixings with noncollective states would be observed.

3. Effect of enlargement of the model space and comparison with experimental data

The first purpose of this paper is to see how the 2γ states calculated in Ref. [4] within a smaller model space are affected by the enlargement of the space. The previous calculation was done in the space up to 2γ basis states. This time I examine that up to 3γ and 4γ basis

states. First, by including 3γ basis states, the upper 2γ band is pushed down by 0.27 MeV ($\omega_{\rm rot} = 0$) – 0.23 MeV ($\omega_{\rm rot} = 0.3$ MeV). Next, by including 4γ, this band is pushed down further by 0.06 – 0.03 MeV. The calculated 0γ and 1γ states are almost unaffected.

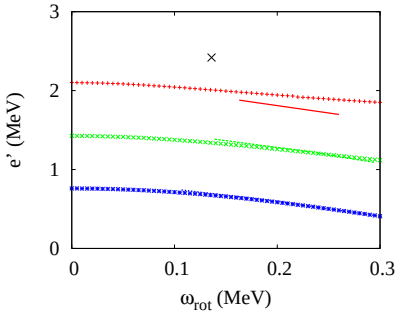

FIG. 5: (Color online) Routhians of calculated 0γ (blue $*$s), 1γ (green $\times$s), and 2γ (red $+$s) states in the $r = -i$ sector of ^{103}Nb are compared with the corresponding data (curves) converted to the rotating frame by using the Harris parameters $\mathcal{J}_0 = 15.45$ MeV^{-1} and $\mathcal{J}_1 = 81.23$ MeV^{-3} that fit the yrast band of ^{104}Mo [22]. The observed transition in band (4), the 3γ candidate, converted to the rotating frame is also shown by a large $\times$.

The final result is presented in Fig. 5. In this nucleus, calculated e'_{2_γ} is still higher, by 0.09 – 0.18 MeV, than the data. See the result for ^{105}Nb below.

B. $0\gamma - 2\gamma$ states in ^{105}Nb

Parameters entering into the calculation are determined in a manner similar to the case of ^{103}Nb. Concretely, the pairing gaps $\Delta_n = 1.05$ MeV and $\Delta_p = 0.85$ MeV, and the deformation $\epsilon_2 = 0.3254$ are adopted conforming to the experimental analyses [15, 21]. The triaxiality $\gamma = -10^\circ$ is chosen to reproduce the observed signature splitting of the ground (0γ) band in the PVC calculation as shown in Fig. 6(a).

The way to determine the quadrupole force strengths is slightly different; those determined to reproduce $\omega_\gamma = 0.7104$ MeV of ^{106}Mo [21] in the reference configuration with $\omega_{\rm rot} = 0$ and $\gamma = 0$ result in a large signature splitting in ω_γ when triaxial deformation is introduced in contrast to the case of ^{103}Nb. Alternatively, they are adjusted so as to reproduce the above ω_γ at $\omega_{\rm rot} = 0$ and $\gamma = -10^\circ$, then $\kappa_0^{(+)}$ is set equal to $\kappa_2^{(+)}$ as in the case of ^{103}Nb. The values for the residual pairing interaction are set to reproduce the adopted

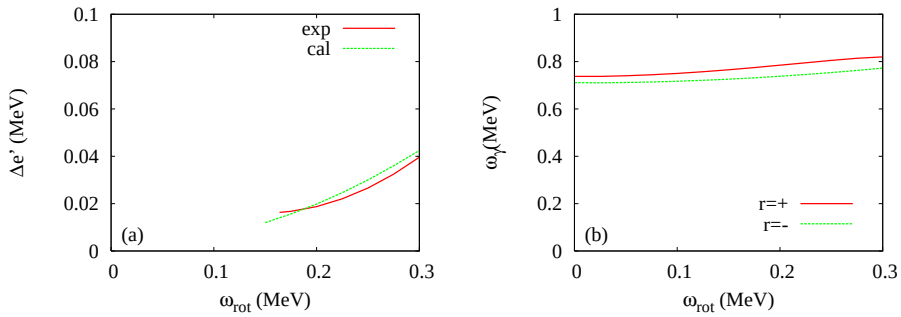

FIG. 6: (Color online) (a) Experimental and calculated signature splitting in the $\pi[422]\,5/2^+$ one-quasiparticle band in ^{105}Nb. Theoretical curve is the result of the particle-vibration coupling calculation. (b) Excitation energies of γ-vibrational RPA phonons in the rotating frame with $r = \pm 1$.

pairing gaps. The obtained $\omega_{\rm rot}$ dependence and the signature splitting of ω_γ are shown in Fig. 6(b).

1. *Distribution of collective states*

In Fig. 7, the distribution of collective states is shown. Overall feature is quite similar to the case of ^{103}Nb but the Routhians of collective solutions are slightly lower reflecting the input ω_γ; this is consistent with the data, see Fig. 7 in Ref. [15]. Other differences from the ^{103}Nb case are that (i) the collectivity of the third strongest 2γ (fifth) state is as low as 30% at around $\omega_{\rm rot} = 0$ but increases as $\omega_{\rm rot}$ increases as seen in Fig. 8, and (ii) among the 3γ states, the lower one is the most collective at $\omega_{\rm rot} = 0.3$ MeV. The latter feature will be discussed below.

2. *Comparison with experimental data*

The characterization of calculated states is done in the same manner as in the case of ^{103}Nb. Then the comparison with the data of 0γ – 2γ states are shown in Fig. 9. In the present case the observed 2γ state is perfectly reproduced in contrast to the ^{103}Nb case in which some deviation remains.

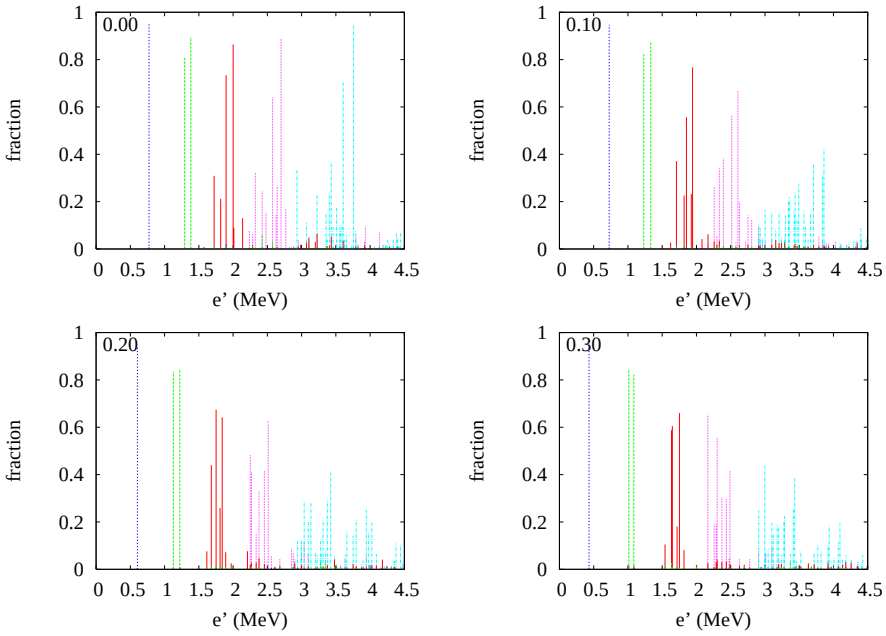

FIG. 7: (Color online) The same as Fig. 1 but for ^{105}Nb.

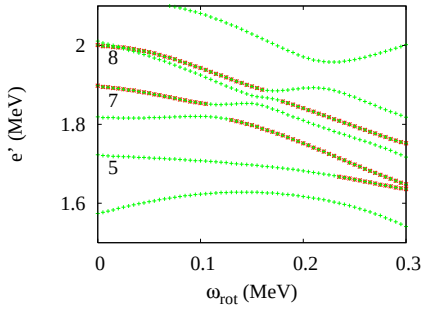

FIG. 8: (Color online) The same as Fig. 2(b) but for ^{105}Nb.

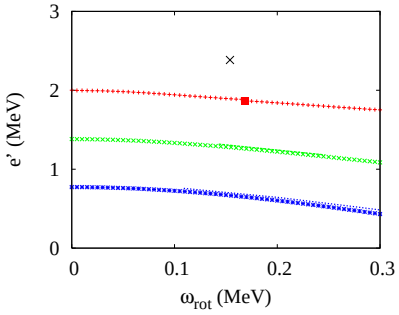

FIG. 9: (Color online) The same as Fig. 5 but for ^{105}Nb. The Harris parameters $\mathcal{J}_0 = 18.08$ MeV^{-1} and $\mathcal{J}_1 = 43.21$ MeV^{-3} that fit the yrast band of ^{106}Mo [21] were used for the conversion.

C. 3γ states in ^{103}Nb and ^{105}Nb

1. *Distribution of collective states*

An issue beyond the scope of Ref. [4] is to characterize the observed band (4) that is conjectured to be a candidate of the 3γ state, the first three-phonon state in deformed nuclei if confirmed.

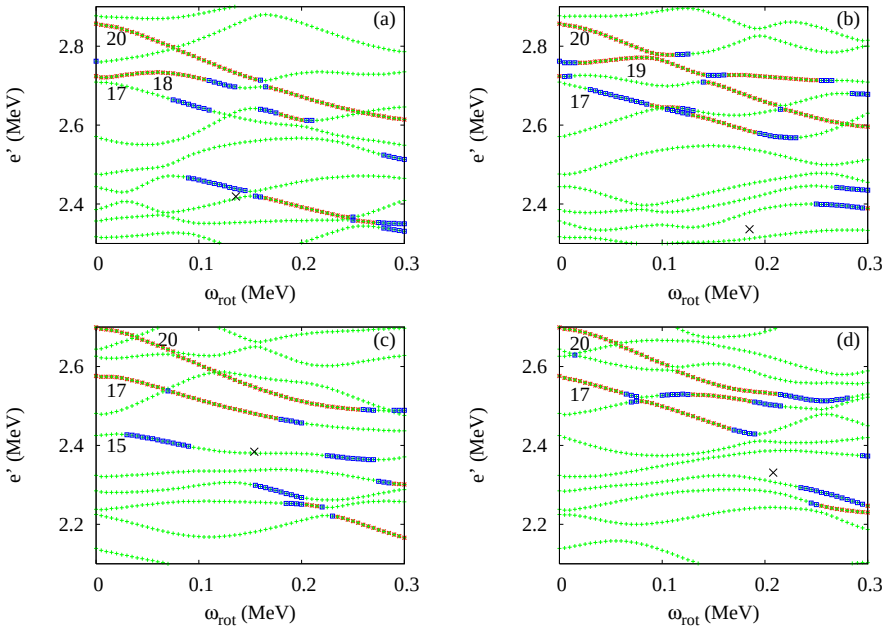

FIG. 10: (Color online) Routians of all calculated PVC states in the regions of 3γ states are shown by green +s as in Figs. 2 and 8. Those with collective fraction more than 50% and 40 – 50% are emphasized by red ×s and blue □s, respectively. (a) $r = -i$ of ^{103}Nb, (b) $r = +i$ of ^{103}Nb, (c) $r = -i$ of ^{105}Nb, and (d) $r = +i$ of ^{105}Nb. The observed transitions in band (4), the 3γ candidate, converted to the rotating frame are also shown by large ×s.

Calculated eigenstates in the region of 3γ states are shown in Fig. 10, (a) ^{103}Nb, favored, (b) unfavored, and (c) ^{105}Nb, favored, (d) unfavored. Contrasting to the previous 1γ and 2γ cases, collective bands are not always parallel, and collectivity tends to move to lower energy states as $\omega_{\rm rot}$ increases. To show this tendency clearly, states with 40 – 50% collective fractions are also marked with blue squares in these figures.

This result can be understood as follows. As discussed already, the highest-lying collective states are the most collective and have the highest K because of the parallel coupling $\Omega + 2n$

for $n\gamma$ states at around $\omega_{\rm rot} = 0$. Because of $K \leq j_{\rm eff}$, where $j_{\rm eff}$ is the effective single-particle angular momentum of particle-vibration coupled states, high-K states have fairly pure high $j_{\rm eff}$. Consequently they feel strong Coriolis force when rotation sets in. Then they start to align their angular momenta to the rotational (x) axis with reducing K, accordingly they reduce their purity and the peak height in Figs. 1 and 7 gradually. This is an aspect of rotational K mixing. Therefore it is expected that the collective 3γ state with K lower than the highest value $\Omega + 6$ would be observed. Actually, the observed band (4) with $K = 9/2$, indicated by large crosses in the figures, sits around the location determined by connecting the most collective states at $\omega_{\rm rot} = 0$ and 0.3 MeV in the case of ^{105}Nb. The situation in ^{103}Nb is to some extent similar, but (i) the lowest collective state at high $\omega_{\rm rot}$ is not collective enough and (ii) the calculated states are located higher overall. More sophisticated calculation would be desired because these observations depend on how band crossings occur and in the present model interband interactions occur at the same $\omega_{\rm rot}$ rather than the same I.

2. Interband $B(E2)$

The observed enhanced $B(E2)$s look to be accounted for primarily by vibrational collectivity, and the above scenario that the collectivity of the twentieth state at $\omega_{\rm rot} = 0$ is observed with a lower K after band crossing(s) can lead to enhanced transitions to the 2γ. Before studying $3\gamma \to 2\gamma$ transitions, I check the results of the generarized intensity relation on $2\gamma \to 1\gamma$ and $1\gamma \to 0\gamma$. Some calculated values for ^{103}Nb that can be compared with the observed $B(E2)$ ratios are shown in Table I. Note here that $Q_{\rm tr} = 0.1944$ eb gives the zero-point amplitude $\gamma_0 = 14°$, defined by $\tan\gamma_0 = \frac{\sqrt{2}Q_{\rm tr}}{Q_0}$ [2], by combining with $Q_0 = \langle {\rm f}|Q_0^{(+)}|{\rm f}\rangle$ =1.090 eb. This is larger than the absolute value of the adopted static triaxial deformation.

First, the calculated values in Table I give $\frac{B(E2{:}15/2^+_{2\gamma}\to 11/2^+_{1\gamma})}{B(E2{:}11/2^+_{1\gamma}\to 7/2^+_{0\gamma})} = 2.46$ and $\frac{B(E2{:}15/2^+_{2\gamma}\to 11/2^+_{1\gamma})}{B(E2{:}13/2^+_{1\gamma}\to 9/2^+_{0\gamma})} = 3.64$, which are very close to the harmonic vibrational values 2.59 and 3.34 in Ref. [8], while the corresponding experimental values are 1.53(16) and 3.45(37), respectively. These show that our PVC model describes the observed values precisely aside from the fact that the experimental $B(E2 : 11/2^+_{1\gamma} \to 7/2^+_{0\gamma})$ is slightly enhanced.

Next, the calculated value, $\frac{B(E2{:}11/2^+_{3\gamma}\to 15/2^+_{2\gamma})}{B(E2{:}11/2^+_{1\gamma}\to 7/2^+_{0\gamma})} = 7.32$, is smaller than the corresponding

TABLE I: Properties of calculated $n\gamma \to (n-1)\gamma$ transitions with $n = 1$, 2, and 3, designated by the labels of intrinsic states, in ^{103}Nb. The moment of inertia, $\mathcal{J} = 32.388$ MeV^{-1}, extracted from the energy of the $I = 9/2$ state in the ground band through $E(I) = \left(I(I+1) - K^2\right)/2\mathcal{J}$, was used.

r	Intr.	I_i	K_i	I_f	K_f	Q_tr (eb)	Q_2 (eb)	$B(E2)$ (e^{2}b^2)
$+i$	$3 \to 1$	11/2	9/2	7/2	5/2	0.1944	0.0044	0.02618
$-i$	$3 \to 1$	13/2	9/2	9/2	5/2	0.1944	0.0043	0.01768
$+i$	$9 \to 3$	15/2	13/2	11/2	9/2	0.2704	0.0067	0.06436
$+i$	$20 \to 9$	11/2	9/2	15/2	13/2	0.3122	0.0116	0.19168

experimental value, 13.5(11), but within a factor of 2. The elementary bosonic property, $\hat{a}|n\rangle = \sqrt{n}\,|n-1\rangle$, is reflected in the intrinsic matrix element, Q_tr, in Table I, such as $\frac{0.3122}{0.1944} = 1.61 \simeq \sqrt{3}$. This is modified by the angular-momentum dependence brought by Q_2, and leads to Q_out in Eq. (9). Finally $B(E2)$ is obtained by multiplying a Clebsch-Gordan coefficient. This means that the calculated value contains some of the enhancement from the angular-momentum effect.

TABLE II: The same as Table I but for ^{105}Nb. The moment of inertia $\mathcal{J} = 31.831$ MeV^{-1} was used.

r	Intr.	I_i	K_i	I_f	K_f	Q_tr (eb)	Q_2 (eb)	$B(E2)$ (e^{2}b^2)
$+i$	$3 \to 1$	11/2	9/2	7/2	5/2	0.1928	0.0087	0.02065
$-i$	$3 \to 1$	13/2	9/2	9/2	5/2	0.1928	0.0085	0.01156
$+i$	$8 \to 3$	15/2	13/2	11/2	9/2	0.2674	0.0125	0.05047
$+i$	$20 \to 8$	11/2	9/2	15/2	13/2	0.3122	0.0185	0.22386
$-i$	$20 \to 8$	13/2	9/2	17/2	13/2	0.3122	0.0185	0.22501

I proceed to ^{105}Nb, in which more conspicuous enhancement of $B(E2)$ is observed. In this case γ_0 is 13° and again larger than $|\gamma|$. The calculated values in Table II give $\frac{B(E2{:}15/2^+_{2_\gamma} \to 11/2^+_{1_\gamma})}{B(E2{:}11/2^+_{1_\gamma} \to 7/2^+_{0_\gamma})} = 2.44$ and $\frac{B(E2{:}15/2^+_{2_\gamma} \to 11/2^+_{1_\gamma})}{B(E2{:}13/2^+_{1_\gamma} \to 9/2^+_{0_\gamma})} = 4.37$, while the corresponding experimen-

tal values are 2.01(24) and 1.94(25), respectively. The calculated values are similar to those of ^{103}Nb but in the experimental ones the magnitude of the denominator is inverted.

For those from the 3γ candidates, the calculated values are $\frac{B(E2{:}11/2^+_{3\gamma}\rightarrow 15/2^+_{2\gamma})}{B(E2{:}11/2^+_{1\gamma}\rightarrow 7/2^+_{0\gamma})} = 10.8$ and $\frac{B(E2{:}13/2^+_{3\gamma}\rightarrow 17/2^+_{2\gamma})}{B(E2{:}13/2^+_{1\gamma}\rightarrow 9/2^+_{0\gamma})} = 19.5$, while the corresponding experimental values are 27.5(33) and 40.5(55). The degree of enhancement increases from ^{103}Nb both in the calculation and in the data. In the calculation, this is caused by a cooperation of increase of the numerator and decrease of the denominator. By close examination, the difference in Q_2, magnified by the angular-momentum factor, $I_{\rm f}(I_{\rm f}+1) - I_{\rm i}(I_{\rm i}+1) - \Delta K(K_{\rm i}+K_{\rm f}) = 6$, produces the difference in the $B(E2)$ in the numerator. Again the differences in the ratios from the data are within factors of 2 – 3. This indicates that the main mechanism of the enhancement of $B(E2)$ is the vibrational collectivity as expected, and the angular-momentum effect is also important for the enhancement. Therefore, from the present analyses, it appears promising that the main component of the observed band (4) is a three-phonon γ vibration although some mixing with states that are not included in the present model would be possible.

IV. CONCLUSIONS

The single- and multi-phonon γ-vibrational states in ^{103}Nb and ^{105}Nb have been studied by using the particle-vibration coupling model based on the cranking model and the random-phase approximation. The calculations have been done in the model space including up to 4γ basis states. This is an extension of the previous calculations including up to 2γ basis states. Analyses of aligned angular momenta and wave functions identified the highest lying among the calculated collective states as the most collective and of the highest $K = \Omega + 2n$ for $n\gamma$ states at $\omega_{\rm rot} = 0$. Then, 1γ and 2γ states have been directly identified with the observed ones and shown to reproduce the observed spectrum precisely. In the case of 3γ states, the Routhian of the $K = \Omega + 6$ state is lowered by strong Coriolis force. Because this alignment process reduces K, the most collective state is expected to be observed as a band with a lower K. Based on this scenario, the interband $B(E2)$s for $n\gamma \rightarrow (n-1)\gamma$ transitions with $n = 1$, 2, and 3 have been calculated by adopting the method of the generalized intensity relation. States with $n = 1$ and 2 were found to reproduce well the observed ones. The calculated $3\gamma \rightarrow 2\gamma$ transition rates have accounted for the observed enhancement of the transitions from the 3γ candidates to 2γ states within factors of 2 – 3, primarily by

the vibrational collectivity and secondly by the angular-momentum effect. These analyses indicate that the main component of the observed band (4) is a three-phonon γ vibration.

---

[1] T. Aumann, P. F. Bortignon, and H. Emling, Nucl. Part. Sci. **48**, 351 (1998).

[2] A. Bohr and B. R. Mottelson, *Nuclear Structure Vol. II* (Benjamin, New York, 1975).

[3] F. Corminboeuf et al., Phys. Rev. Lett. **84**, 4060 (2000).

[4] M. Matsuzaki, Phys. Rev. **C83**, 054320 (2011).

[5] H. J. Li et al., Phys. Rev. **C87**, 057303 (2013).

[6] J. C. Durand and R. Piepenbring, Phys. Rev. **C54**, 189 (1996).

[7] H. B. Ding et al., Phys. Rev. **C74**, 054301 (2006).

[8] J. -G. Wang et al., Phys. Lett. **B675**, 420 (2009).

[9] G. Long et al., Chin. Phys. Lett. **26**, 092502 (2009).

[10] J. A. Sheikh, G. H. Bhat, Y. Sun, and R. Palit, Phys. Lett. **B688**, 305 (2010).

[11] D. R. Jensen et al., Phys. Rev. Lett. **89**, 142503 (2002).

[12] G. Schönwaßer et al., Phys. Lett. **B552**, 9 (2003).

[13] M. Matsuzaki and S. -I. Ohtsubo, Phys. Rev. **C69**, 064317 (2004).

[14] Y. R. Shimizu, M. Matsuzaki, and K. Matsuyanagi, Phys. Rev. **C72**, 014306 (2005).

[15] H. J. Li et al., Phys. Rev. **C88**, 054311 (2013).

[16] M. Matsuzaki, Y. R. Shimizu, and K. Matsuyanagi, Prog. Theor. Phys. **77**, 1302 (1987); *ibid.* **79**, 836 (1988).

[17] M. Matsuzaki, Nucl. Phys. **A491**, 433 (1989); *ibid.* **A519**, 548 (1990).

[18] G. Gervais et al., Nucl. Phys. **A624**, 257 (1997).

[19] M. Matsuo and K. Matsuyanagi, Prog. Theor. Phys. **74**, 1227 (1985); *ibid.* **76**, 93 (1986); *ibid.* **78**, 591 (1987).

[20] Y. R. Shimizu and T. Nakatsukasa, Nucl. Phys. **A611**, 22 (1996).

[21] A. Guessous et al., Phys. Rev. Lett. **75**, 2280 (1995).

[22] A. Guessous et al., Phys. Rev. **C53**, 1191 (1996).